Assessing the sensitivity of diffusion MRI to detect neuronal activity directly

Ruiliang Bai[a,b], Craig V. Stewart[c], Dietmar Plenz[c], and Peter J. Basser[a,1]

[a]Section on Quantitative Imaging and Tissue Science, Division of Imaging, Behavior and Genomic Integrity, Eunice Kennedy Shriver National Institute of Child Health and Human Development, National Institutes of Health, Bethesda, MD 20892; [b]Biophysics Program, Institute for Physical Science and Technology, University of Maryland, College Park, MD 20740; and [c]Section on Critical Brain Dynamics, Laboratory of Systems Neuroscience, National Institute of Mental Health, National Institutes of Health, Bethesda, MD 20892

Edited by Marcus E. Raichle, Washington University in St. Louis, St. Louis, MO, and approved February 2, 2016 (received for review October 8, 2015)

Functional MRI (fMRI) is widely used to study brain function in the neurosciences. Unfortunately, conventional fMRI only indirectly assesses neuronal activity via hemodynamic coupling. Diffusion fMRI was proposed as a more direct and accurate fMRI method to detect neuronal activity, yet confirmative findings have proven difficult to obtain. Given that the underlying relation between tissue water diffusion changes and neuronal activity remains unclear, the rationale for using diffusion MRI to monitor neuronal activity has yet to be clearly established. Here, we studied the correlation between water diffusion and neuronal activity in vitro by simultaneous calcium fluorescence imaging and diffusion MR acquisition. We used organotypic cortical cultures from rat brains as a biological model system, in which spontaneous neuronal activity robustly emerges free of hemodynamic and other artifacts. Simultaneous fluorescent calcium images of neuronal activity are then directly correlated with diffusion MR signals now free of confounds typically encountered in vivo. Although a simultaneous increase of diffusion-weighted MR signals was observed together with the prolonged depolarization of neurons induced by pharmacological manipulations (in which cell swelling was demonstrated to play an important role), no evidence was found that diffusion MR signals directly correlate with normal spontaneous neuronal activity. These results suggest that, whereas current diffusion MR methods could monitor pathological conditions such as hyperexcitability, e.g., those seen in epilepsy, they do not appear to be sensitive or specific enough to detect or follow normal neuronal activity.

diffusion MRI | functional | neuronal activity | organotypic culture | intracellular calcium

Developing a direct MRI method to detect neuronal activity in vivo and noninvasively is a major focus in neuroscience. Progress in this area is required to improve our understanding of normal brain function, and in a clinical setting, to develop new tools for studying normal and abnormal development to diagnose diseases and disorders of the brain. Functional MRI (fMRI) has been widely used in the cognitive neurosciences since its invention in the 1990s (1–3). The most widely used fMRI method, blood-oxygenation-level-dependent (BOLD) MRI, detects hemodynamic changes in the brain, which only indirectly reflects neuronal activity. Moreover, its hemodynamic origin limits both its spatial and temporal resolution and its interpretation as a direct proxy for neuronal activity (4, 5).

More recently, several MRI methods were proposed to provide more direct measures of neuronal excitation (6). In particular, diffusion MRI, a method to measure the apparent diffusivity of water within tissues (7–9), has been suggested as a direct functional imaging method to detect neuronal activity (10–13). Early in vivo experiments in both humans and animals reported small but significant increases in highly diffusion-weighted MRI signals, which were ascribed to changes directly induced by the underlying neuronal activity rather than indirect hemodynamic changes (10–13). In vitro experiments on brain slices (14, 15) and spinal cord (16) reported similar reductions in water diffusivity under conditions of extreme hyperexcitability using strong pharmacologic stimulants.

However, functional diffusion MRI (fDMRI) has not been widely used or adopted since its introduction almost two decades ago. Two major reasons for this may be a dearth of experiments that convincingly establish its neurophysiological basis and the poor reproducibility of the originally reported changes in diffusion MRI signals by different laboratories. The inability to detect the predicted changes using fDMRI and the possible confounds of hemodynamic contributions in fDMRI measurements in vivo do not argue for a robust connection between changes in diffusion MRI and underlying neuronal activity (17–20). Thus, "ground-truth" experiments, potentially establishing a connection between the changes in diffusion MRI and underlying neuronal activity, are needed, particularly to shed light on the possible biophysical basis of the fDMRI signal.

Recently, we developed a novel test bed that could be used to assess non–hemodynamic-based functional MRI methods, in which MR signal acquisition and intracellular calcium fluorescence imaging to monitor neuronal activity can be performed simultaneously on organotypic cortical cultures from rat brains (21). The organotypic cortex culture is a well-characterized biological model of neuronal activity free of hemodynamic, respiratory, and other physiological confounds. Not only is the in vivo cortical cytoarchitecture preserved (including cortical layers and cortical cell types), but neuronal activity in the culture also displays bursts of spontaneous neuronal avalanches grouped into so-called up-states and separated by periods of low activity (22–25), resembling resting neuronal activity in vivo (26–28). Specifically, fluorometric calcium (Ca^{2+}) imaging is used to detect intracellular Ca^{2+} concentration changes that closely follow action potentials in neurons under

Significance

Diffusion functional MRI has been proposed as a noninvasive neuroimaging method to detect neuronal activity more directly than current blood-oxygen-level-dependent functional MRI, yet initial findings have proven difficult to interpret and reproduce. Here, we study the direct relationship between water diffusion and neuronal activity by simultaneously imaging intracellular calcium using fluorescence along with diffusion MR acquisitions from organotypic rat brain cortex cultures. Although we found that diffusion MR methods can follow the pathological time course of hyperexcitability, e.g., as those seen in epilepsy, they do not appear to be sensitive or specific enough to detect or follow normal neuronal activity.

Author contributions: R.B., D.P., and P.J.B. designed research; R.B. performed research; R.B. and C.V.S. contributed new reagents/analytic tools; R.B. analyzed data; R.B., D.P., and P.J.B. wrote the paper; and P.J.B. supervised the project.

The authors declare no conflict of interest.

This article is a PNAS Direct Submission.

[1]To whom correspondence should be addressed. Email: pjbasser@helix.nih.gov.

This article contains supporting information online at www.pnas.org/lookup/suppl/doi:10.1073/pnas.1519890113/-/DCSupplemental.

normal conditions and provide a direct method for detecting neuronal spiking activity in a neuronal network (29, 30). This test bed thus allows one to study precisely and accurately temporal correlations between the candidate functional MR signals, which are free of the usual in vivo confounds, and the underlying neuronal spiking activity by using an independent intracellular Ca^{2+} imaging experiment (21).

In the current study, diffusion MR signals are obtained simultaneously with intracellular calcium fluorescence imaging of the organotypic cortex culture. The direct effects of neuronal activity on the diffusion MR signals are studied by time-series analysis of the simultaneous calcium and MR signals during normal neuronal activity and in different pathological states, which include induced hyperexcitability by kainic acid (kainate) and potassium, disinhibition by picrotoxin (PTX), suppression of excitability by tetrodotoxin (TTX), and cell volume modulation caused by osmotic pressure challenges. On the basis of these findings, it is possible to assess the prospect of detecting normal and abnormal neuronal activity using fDMRI and to better understand the relationship between fDMRI changes and biophysical mechanisms associated with neuronal excitation.

Results

In vitro calcium imaging was performed using 50 μM Oregon Green 488 BAPTA-1 (OGB; Life Technologies) under a modified macrozoom fluorescence microscope (MVX10 MacroView; Olympus) mounted above the tissue specimen. Diffusion MR measurements were performed with a static gradient spin echo NMR sequence using a single-sided NMR profiling system (21, 31). For the diffusion MR acquisition, five b-values (b = 0, 600, 1,200, 1,800, and 2,400 s/mm^2) with TR = 2 s and two-step phase cycling were used. The diffusion MR signal, S, was well fitted by a four-parameter bicomponent model (10, 14, 15, 32–35)

$$S(b) = S_0\left[(1-f)\exp\left(-bD_{\text{fast}}\right) + f\exp(-bD_{\text{slow}})\right], \qquad [1]$$

where D_{fast} and D_{slow} are the diffusion coefficients of the slow and fast diffusion components, respectively, f is the slow diffusion component fraction, and S_0 is the MR signal without diffusion weighting. More details about this methodology can be found in ref. 21 and in *Materials and Methods*.

At first, we induced hyperexcitability in the cortex cultures by bath perfusion with a high concentration of kainate (100 μM) or extracellular potassium chloride (30 mM) following a protocol adapted from ref. 14. Kainate induces hyperexcitability by activating glutamate receptors (glutamate is an excitatory neurotransmitter in the CNS), whereas an increase in extracellular potassium (K^+) excites neurons directly by depolarizing their intracellular resting membrane potential. The concentration dependence of the kainate effect was further studied. We also studied spontaneous neuronal activity under conditions of disinhibition, i.e., when fast synaptic inhibition was reduced with the gamma-aminobutyric acid ($GABA_A$) receptor channel blocker, PTX (5 μM and 50 μM). For controls, we suppressed neuronal spiking by blocking sodium channel permeability using TTX (0.2 μM). Two statistical time-series analysis methods were used to study the potential effect of a single event of the normal spontaneous neuronal activity on diffusion-weighted MR signals at a temporal resolution of 100 ms. Finally, we conducted osmotic pressure experiments to test possible effects of cell swelling and deswelling on changes in diffusion MR signals during the depolarization block.

Depolarization Block by Kainate. Normal artificial cerebrospinal fluid (ACSF) perfusion (~30 mL/h) was followed by 10 min of perfusion with 100 μM kainate added, followed by a washout with normal ACSF (Fig. 1). Care was taken to maintain constant perfusion flow rate, temperature, and oxygenation of the ACSF to minimize perfusion artifacts. As shown in Figs. 1*A* and 2*A*, during normal activity, the population aggregate intracellular calcium signal (F) was characterized by brief (0.5–3 s) and irregular periods of neuronal excitation (21, 28) separated by ~10 s of very low activity. Within 2–3 min of kainate perfusion (including the perfusate switching time), a strong increase in F and then a change to a prolonged plateau was observed, followed by a recovery close to the predrug baseline levels during washout. The plateau in F indicates strong excitation of the neuronal population including potentially a depolarization block throughout the spatial extent of the culture (Fig. 1*B*).

In this experiment, three of the four diffusion MR fitting parameters (Eq. **1**) during normal activity, i.e., before kainate perfusion, are as follows: $f = 8.01 \pm 1.68\%$, $D_{\text{fast}} = 2.65 \pm 0.04$ μm^2/ms, and $D_{\text{slow}} = 0.20 \pm 0.05$ μm^2/ms (all $n = 6$ samples, mean ± SEM here and in the following text). The diffusion MR signals changed almost simultaneously and similarly in scale with F, the intracellular calcium signal. In the example shown in Fig. 1*A*, the slow diffusion component fraction f increased from 8.47% before drug application to 10.38% during the kainate application. In all cultures scanned, increases of the diffusion MR signal at higher b-values were observed during kainate perfusion, and they increased with higher b-values: −0.86 ± 0.68% ($P = 0.87$) at b = 0 s/mm^2, 3.29 ± 1.06% ($P < 0.01$) at b = 600 s/mm^2, 11.2 ± 1.6% ($P < 0.0005$) at b = 1,200 s/mm^2, 17.5 ± 2.0% ($P < 0.0005$) at b = 1,800 s/mm^2, and 11.9 ± 5.7% ($P < 0.05$) at b = 2,400 s/mm^2 (Fig. 1*D*). The smaller-than-expected change at b = 2,400 s/mm^2 might be artifact due to its low signal-to-noise ratio (SNR). Similarly, the slow diffusion component fraction f increased significantly by 20.1 ± 3.4% ($P < 0.001$) with respect to the predrug levels (Fig. 1*E*). The changes in diffusion MR signals agree with the previous work on acute rat cortical slices (14), although no simultaneous monitoring of neuronal activity with well-characterized method was performed. Here and in the following sections, all of the P values were obtained by paired Student's t test for drug and predrug data. During ACSF washout, the diffusion MR changes also returned to near predrug levels as did the calcium signal.

Dependence of Diffusion MR Signal on Kainate Concentration. The observed prolonged depolarization when using 100 μM kainate was directly related to the level of neuronal excitation in the cultures as shown by its concentration dependency. As shown in Fig. 2*A*, when kainate was used at lower concentrations than 100 μM, signal levels dropped accordingly. At 10 μM, the prolonged depolarization was still apparent but smaller than that at 100 μM kainate with an increase in spontaneous population events. At 1 μM, the prolonged depolarization level was smaller than that at 10 μM kainate; however, an increase in normal population events was clearly visible in Fig. 2*A*. We quantified the change in the calcium fluorescence baseline (F_0, representative of the prolonged depolarization level; see details in *Materials and Methods*) as a function of kainate as 41.7 ± 10.9% at 100 μM kainate, to 26.3 ± 5.9% ($n = 6$) at 10 μM kainate and 4.9 ± 11.6% ($n = 6$) at 1 μM kainate (Fig. 2*B*). Importantly, changes in diffusion MR signal similarly depended on the kainate concentration. For instance, the increase of the diffusion MR signals (average of the MR signals at b = 1,800 and 2,400 s/mm^2) dropped from 14.7 ± 3.3% ($P < 0.005$) at 100 μM kainate to 4.50 ± 2.19% ($P < 0.05$) at 10 μM kainate and 2.88 ± 1.26% ($P = 0.036$) at 1 μM kainate. The changes in the slow diffusion component fraction $\Delta f/f_0$, decreased from 20.1 ± 3.4% ($P < 0.001$) at 100 μM kainate to 6.34 ± 1.30% ($P < 0.005$) at 10 μM kainate and 2.47 ± 1.44% ($P = 0.07$) at 1 μM kainate.

Diffusion MR Signals in Response to High Extracellular K^+ Concentration. To verify the effect of the depolarization block on the diffusion MR signals, extracellular K^+ concentration was increased to

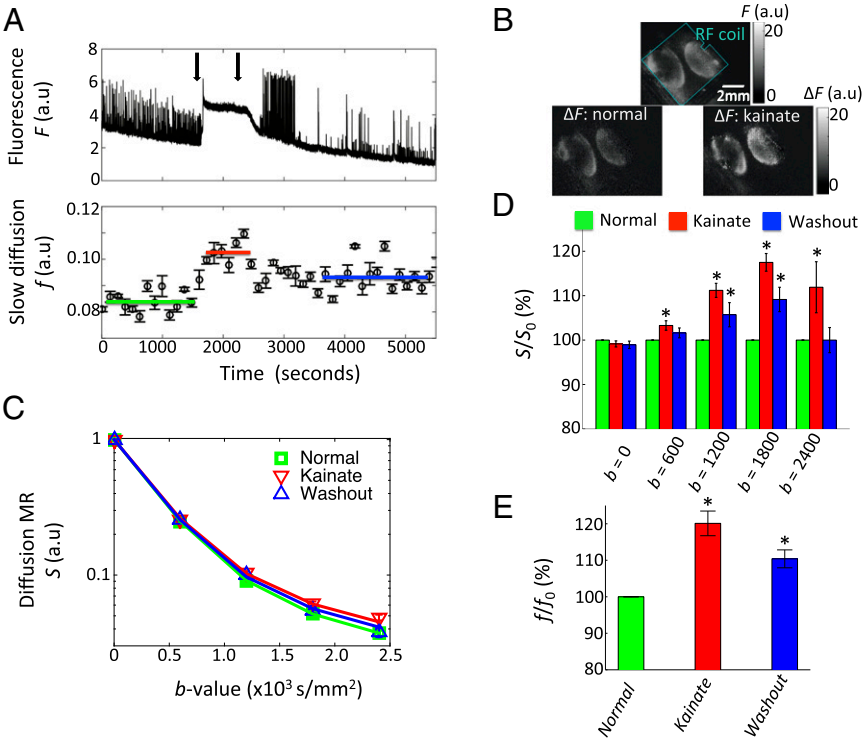

Fig. 1. Prolonged depolarization with kainate. (*A*) The intracellular calcium fluorescence signal (*F*) integrated over the entire neuronal population (*Upper*) and the slow diffusion component fraction (*f*) derived from modeling the diffusion MR signal (*Lower*; data average every 2 min). Colored continuous curve: data average in each phase. The two black arrows indicate the start of the 100 μM kainate perfusion (*Left*) and the washout with ACSF (*Right*). (*B*) (*Upper*) Large-field image of an organotypic cortex culture (two cortex slices positioned close to each other) stained with OGB-1 under fluorescence illumination within the RF coil. (*Lower*) Image of fluorescence changes with respect to the baseline under normal neuronal activity and kainate-induced prolonged depolarization. (*C*) The averaged diffusion MR signals (*S*) in *A* during three phases: prekainate normal neuronal activity, kainate perfusion, and ACSF washout. Continuous curves are obtained from model fits. (*D* and *E*) The statistical results ($n = 6$) of the normalized diffusion MR signals (*D*) and the normalized slow diffusion component fraction (*E*) during three phases: prekainate normal neuronal activity, kainate perfusion, and ACSF washout. In both *D* and *E*, the results were normalized with the results from the prekainate normal activity. $^*P < 0.05$ with Student's *t* test for MR results.

induce prolonged depolarization via a different mechanism than kainate. A strong depolarization effect similar to that for kainate was observed during 10 min of perfusion with 30 mM potassium chloride (KCl) containing ACSF (Fig. 3*A*). The calcium baseline (F_0) increased by 72.0 ± 6.0% compared with the predrug baseline in all cultures ($n = 4$; Fig. 3*B*). The changes in diffusion MR signals were found to be simultaneous to the calcium signal changes during high-concentration K^+ perfusion. For example, the diffusion MR signal (the average of MR signals at $b = 1{,}800$ and 2,400 s/mm^2 increased by 9.71 ± 2.19% ($P < 0.05$) and the slow diffusion component fraction f also increased by 11.4 ± 2.4% ($P < 0.005$) compared with the predrug values. The changes in diffusion MR signals also agree with the previous work on acute rat cortical slices with diffusion MRI only (14). During the washout, both calcium signals and diffusion MR signals recovered back up toward predrug levels.

Diffusion MR Signals from Disinhibited Neuronal Activity. Unlike the direct depolarization induced by kainate or an increase in extracellular potassium concentration, PTX enhances neuronal activity by reducing inhibitory synaptic transmission in neuronal networks, which leads to prolonged periods of synchronized neuronal activity. Similar to what was found for the concentration dependency of kainate-induced neuronal activity, we found a dose dependence for PTX. At 5 μM PTX, synchronized neuronal activity was increased as indicated by a decrease of the frequency of spontaneous population events but an increase of their amplitude as seen in calcium imaging (Fig. 4*A*) (25, 36). There were no significant changes in either the diffusion MR signals or the slow diffusion component fraction during the 5 μM PTX application ($n = 5$; Fig. 4*B*). At a higher concentration (50 μM), prolonged depolarization represented as a slight increase (32.0 ± 17.6%) in the calcium baseline signal intensity following the PTX perfusion was observed within 2–3 min. Importantly, at this high concentration, both the highly diffusion weighted MR signals (the average of MR signals at $b = 1{,}800$ and 2,400 s/mm^2) and the slow diffusion component fraction f showed significant increases ($n = 4$): 5.95 ± 0.29% ($P < 0.0005$) and 7.07 ± 0.16% ($P < 0.0001$), respectively.

Suppression of Normal Spontaneous Activity by TTX Does Not Affect the Diffusion MRI Signal. Spiking activity was suppressed in the organotypic culture by adding 0.2 μM TTX to the bath to assess whether the MR diffusion signal contains contributions from normal spontaneous neuronal activity. Within 1–3 min of TTX application, neuronal activity was almost completely suppressed with the number of neuronal events per minute dropping from 12.0 ± 1.7 to 0.22 ± 0.12 (Fig. 5*A*). Some neuronal activity was recovered during washout as expected for this drug ($n = 6$; Fig. 5*B*). No significant changes were found in either the diffusion MR signals or the slow diffusion component fraction during the application of 0.2 μM TTX (Fig. 5*C*), where the changes were 1.06 ± 2.09% ($P = 0.68$) for the diffusion-weighted MR signal (the average of MR signals at $b = 1{,}800$ and 2,400 s/mm^2) and 1.33 ± 2.07% ($P = 0.73$) for the slow diffusion component fraction. This set of experiments demonstrated that the diffusion MR signal is not sensitive to the level of normal spontaneous neuronal activity.

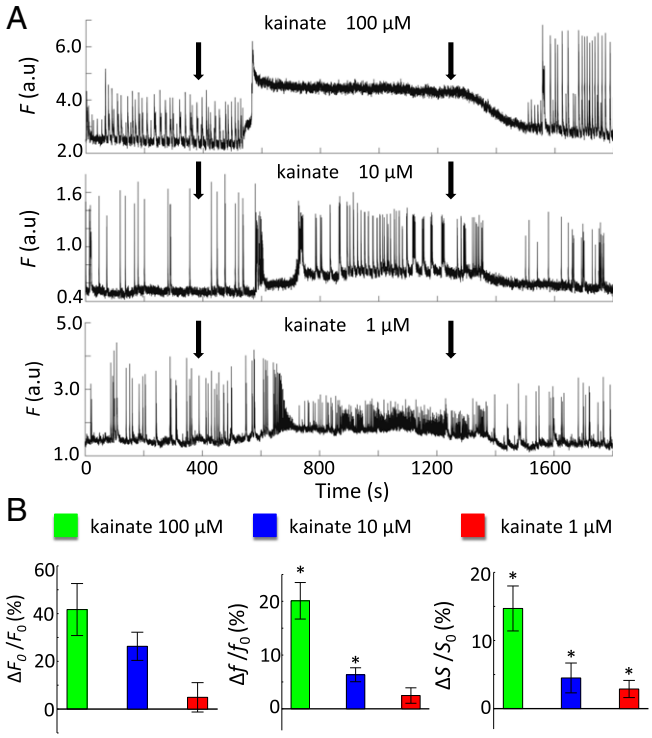

Fig. 2. Dependence of kainate concentration. (*A*) The population of the intracellular calcium fluorescence signal (*F*) in response to 10 min of kainate perfusion at three concentrations: 100 (*Top*), 10 (*Middle*), and 1 μM (*Bottom*). The two black arrows in each subplot of *A* are the start of the kainate perfusion (*Left*) and washout with ACSF (*Right*), respectively. (*B*) The normalized changes in the fluorescence baseline (F_0, *Left*), the slow diffusion component fraction (*Center*), and the diffusion MR signals (the average of MR signals at b = 1,800 and 2,400 s/mm^2; *Right*) under kainate perfusion with various kainate concentrations. *P < 0.05 with Student's t test for MR signals.

Time-Series Analysis Indicates Diffusion MR Signals Are Unaffected by Each Single Event of Normal Spontaneous Neuronal Activity. To further confirm that each single event of the normal spontaneous neuronal activity does not affect the diffusion MR signals, time-series analysis of the heavily diffusion-weighted MR signals (b = 1,800 s/mm^2) and calcium signals were performed on 16 organotypic cortical cultures in control experiments without a pharmacologic intervention. Periods of high ("active") and low ("resting") neuronal activity were identified in the intracellular calcium signal, and the MR signal was binned into these two categories on the basis of its relative recording time under two types of hypothesis as illustrated in Fig. 6 *A* and *B*. In the paired comparison of the diffusion-weighted signals in active and resting states, no significant evidence was found that each single event of normal spontaneous neuronal activity would affect the highly diffusion-weighted MR signals at a temporal resolution of 100 ms under either hypothesis (Fig. 6 *C* and *D*).

Effects of Osmotic Pressure During Depolarization Block. It has been speculated that previously observed functional diffusion MR changes during prolonged depolarization were the result of cell swelling (33). To investigate this hypothesis, the ACSF osmotic pressure was modulated during perfusion of normal ACSF (control) and ACSF with 100 μM kainate. Cell swelling and shrinkage were expected under conditions of hypoosmotic and hyperosmotic pressure, respectively (37). In the control (without kainate), a significant reduction (P < 0.05) of both the diffusion-weighted MR signal (the average of the MR signals at b = 1,800 and 2,400 s/mm^2, −5.75 ± 1.25%, n = 4) and f (−4.84 ± 1.71%) was observed at +80 mOsm, whereas a significant increase (P < 0.005) of both parameters (15.2 ± 1.8% and 14.6 ± 1.7%, respectively) was observed at −80 mOsm (Fig. 7*A*). Spontaneous activity shown in the calcium signal also changed (reduction in either the firing rate or the amplitude of the spontaneous spikes) in the osmotic pressure challenge experiments, but recovered close to the preosmotic stress induced states as the diffusion MR signals during washout with normal ACSF (Fig. S1).

In the kainate experiments with a +80-mOsm osmotic pressure challenge, the calcium signal still showed a strong depolarization during the kainate application under +80 mOsm (Fig. S2). However, the change in highly diffusion-weighted MR signals (average at b = 1,800 and 2,400 s/mm^2) was significantly reduced (P < 0.01, n = 4) from 14.7 ± 3.3% (no osmotic pressure challenge) to 1.39 ± 1.42% by the osmotic pressure challenge, as was the change in the slow diffusion component fraction f (P < 0.005) from 20.1 ± 3.4% to 1.60 ± 0.92% (Fig. 7*B*). During the subsequent washout with normal ACSF, the depolarization was reduced, whereas some spontaneous activity appeared (Fig. S2). Furthermore, the application of a second 100 μM kainate perfusion without osmotic pressure challenge following the 30-min washout also showed much higher increases in both the diffusion-weighted MR signals (averages at b = 1,800 and 2,400 s/mm^2, 11.7 ± 1.7%, P < 0.005) and the slow diffusion component fraction f (10.1 ± 1.1%, P < 0.001) than the first 100 μM kainate perfusion with +80 mOsm ACSF (Fig. S2).

Diffusion MR in a Pathological Stroke Model via Oxygen/Glucose Deprivation. A reduced water apparent diffusion coefficient (ADC) has also been reported in other pathological states, such as stroke (38, 39). Diffusion MRI is the gold standard neuroimaging method to diagnose occlusive stroke clinically, reliably producing an

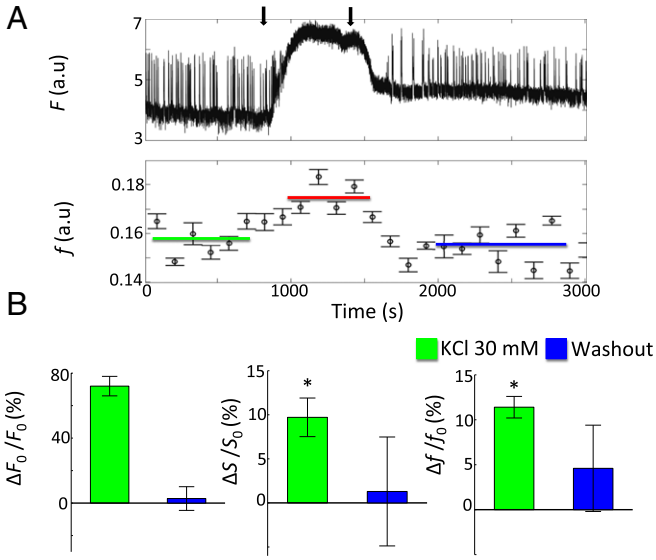

Fig. 3. The effects of high-concentration extracellular K^+. (*A*) An example of the population of the intracellular calcium fluorescence signal (*Upper*) and the slow diffusion component derived from modeling the diffusion MR signal (*Lower*; data average at every 2 min) in response to a 10-min perfusion of 30 mM KCl in ACSF. Colored continuous curve: data average in each phase. The two black arrows indicate the start of drug perfusion (*Left*) and washout with normal ACSF (*Right*), respectively. (*B*) The normalized changes in the fluorescence baseline (*Left*), the diffusion MR signals (the average of MR signals at b = 1,800 and 2,400 s/mm^2; *Center*), and the slow diffusion component fraction (*Right*) under perfusion of the ACSF with 30 mM KCl and washout with normal ACSF. *P < 0.05 with Student's t test for MR signals.

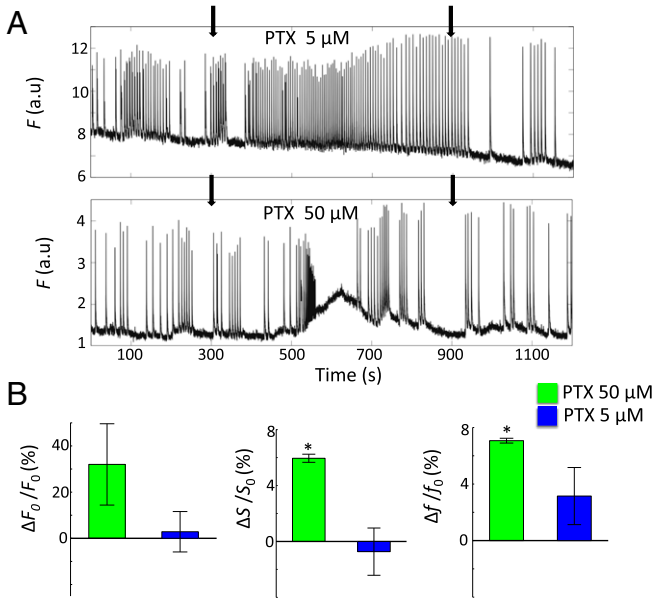

Fig. 4. Disinhibition modulation. (*A*) Calcium fluorescence signal in response to 10-min PTX perfusion studies with two concentrations: 5 (*Upper*) and 50 μM (*Lower*). The two black arrows are the starting times of the PTX perfusion (*Left*) and washout with ACSF (*Right*). (*B*) The normalized changes in the fluorescence baseline (*Left*), the diffusion MR signals (the average of MR signals at b = 1,800 and 2,400 s/mm^2, *Center*), and the slow diffusion component fraction (*Right*) during PTX perfusion with various PTX concentrations. *P < 0.05 with Student's t test for MR signals.

increased diffusion-weighted signal and a concomitant reduction in the ADC in ischemic areas (40, 41). Another phenomenon associated with ischemia caused by acute stroke is depolarization of the cell membrane and calcium uptake by neurons (42, 43). To assess the effects of these two phenomena, a stroke model using an oxygen/glucose deprivation (OGD) protocol was tested (37, 41, 44). In the OGD protocol, the glucose was deprived (NaCl was added to maintain constant osmotic pressure) and the ACSF was kept saturated with 95% N_2 + 5% O_2. The OGD started with a fast perfusion speed (60 mL/h) for 15 min to remove oxygen and glucose from the chamber quickly, and then the perfusion was returned to normal speed (30 mL/h) for another 2 h.

An increase in the baseline of F with normal neuronal spikes suppressed was observed as the OGD started in all of the admissible samples (n = 3) until the photo-bleaching effect appeared (Fig. 8*A*). The washout with normal ACSF did not restore the normal neuronal activity. In the control (normal ACSF perfusion), normal neuronal activity took place during the entire 2.5-h recording period. In diffusion MR, the diffusion-weighted MR signals also started increasing as the OGD began, whereas the control showed no significant changes. As shown in Fig. 8 *A* and *C*, greater increases of the diffusion-weighted MR signals were observed at higher b-values and longer OGD perfusion times. The washout did not result in recovery of the diffusion signal back to the pre-OGD levels. The ADC was calculated at b = 1,800 s/mm^2 with the equation

$$ADC = -\frac{1}{b}\exp\left[\frac{S(b)}{S(b=0)}\right]. \quad [2]$$

The ADC started from 1.35 ± 0.08 mm^2/s in the pre-OGD state and dropped by 4.99% at the first 30-min OGD perfusion and kept decreasing until it reached 14.9% at the end of the 2-h OGD perfusion. The washout did not recover the ADC either.

Discussion

The debate about whether diffusion MRI can detect neuronal activity more directly and accurately than conventional hemodynamic-based fMRI methods has never stopped since it was proposed (10–20). Our hybrid test bed, which allows for simultaneous monitoring of neuronal activity via intracellular calcium fluorescence imaging during MR acquisition on the organotypic cortical cultures, provides a unique opportunity for direct, time-dependent comparisons of the diffusion MR signals with neuronal activity without any hemodynamic or other physiologic confounds. Our results with this fMRI test bed suggest that the highly diffusion-weighted MR signals were only sensitive to pathological hyperexcitability (prolonged cell membrane depolarization), but were independent of, and insensitive to, the level of the normal neuronal population activities (spikes).

In this study, significant increases of the highly diffusion-weighted MR signals were observed under depolarization block induced by high-concentration kainate, extracellular K^+, and PTX. Kainate is a potent analog of glutamic acid, which is the principal excitatory neurotransmitter in the CNS. An application of high concentration kainate can cause prolonged depolarization of the cell membrane accompanying an influx of Ca^+ (45, 46); this phenomenon was clearly demonstrated in Fig. 1*A*. High-concentration extracellular K^+ can also induce cell depolarization by changing the ion gradients across the cell membrane (47), as shown in Fig. 3*A*. The $GABA_A$ receptor chloride channel blocker PTX was also shown to depolarize the cell at high concentrations in Fig. 4*A* and ref. 24. In all three conditions, emergence of a "plateau"—a depolarization in the calcium signal—was observed. These plateaus represent sustained periods of high activity associated with spike recession and depolarization block as described previously in these culture systems (24). Synchronous with this abnormal activity, the

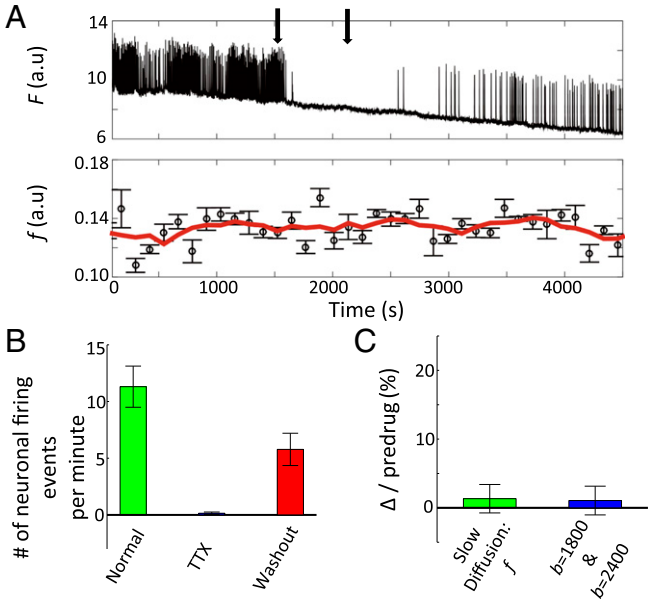

Fig. 5. Neuronal activity suppression with TTX. (*A*) Examples of the population of the intracellular calcium fluorescence signal (*Upper*) and the slow diffusion component derived from modeling the diffusion MR signal (*Lower*, data average every 2 min) in response to a 10-min perfusion of 0.2 μM TTX in ACSF. Red continuous curve: sliding average (six data points each). The two black arrows indicate the start of the drug perfusion (*Left*) and washout with normal ACSF (*Right*), respectively. (*B*) The change in the number of neuronal firing events per minute under perfusion of normal ACSF, 0.2 μM TTX, and washout with normal ACSF. (*C*) The normalized changes in the slow diffusion component fraction f and the diffusion MR signals (the average of MR signals at b = 1,800 and 2,400 s/mm^2) during perfusion of 0.2 μM TTX.

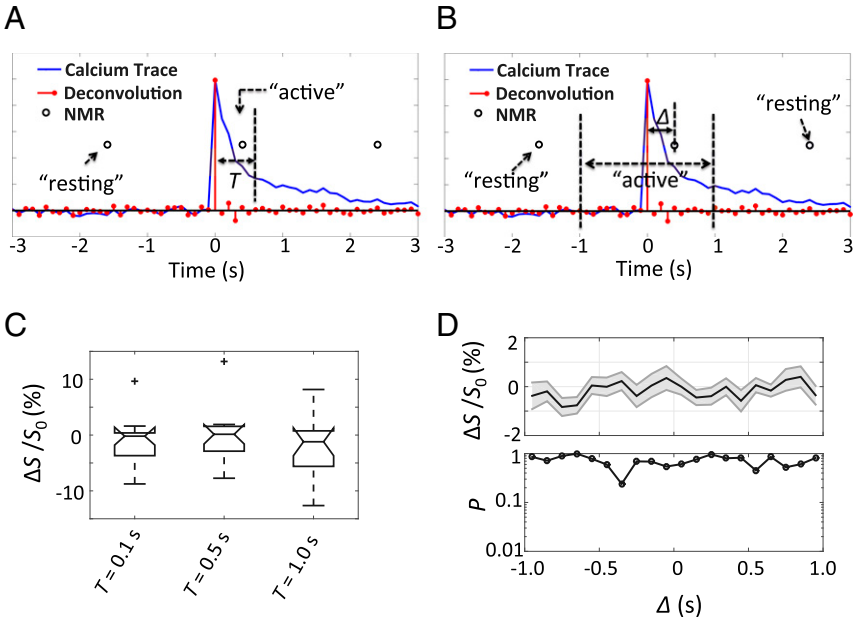

Fig. 6. Control experiments: time-series analysis of the calcium signal and diffusion MR signal without a pharmacologic intervention. (*A* and *B*) Schematic diagram of two types of hypothesis: (*A*) Type 1: each neuronal population activity event would only affect the diffusion MR signal (active) recorded immediately after it within a time window, *T*, which was varied over a range from $T = 0.1$ to 1.0 s in steps of 0.1 s; and (*B*) Type 2: each neuronal population activity event would only affect the MR signal (active) recorded within 1 s before and following it. The active MR signals were further binned into groups on the basis of how separated they were in time (*Δ*) from the neuronal event with a time step of 0.1 s. (*C*) The boxplots of statistical results of the changes in the active state with respect to the resting diffusion MR signals (S_0) in Type 1 analysis at time windows 0.1, 0.5, and 1.0 s. For display purposes, some outliers were not plotted. (*D*) The time profiles of the changes in the active state with respect to the resting diffusion MR signals (S_0) in Type 2 analysis and their corresponding *P* values with Student's *t* test. The black line is the mean, and the light shadow is the mean SE in *D*, *Upper*.

diffusion-weighted MR signals showed significant increases; this change became larger as the *b*-values increased. In other words, the slow diffusion component fraction showed significant increases in the bicomponent model. The simultaneous responses in both the diffusion MR signals and intracellular calcium signals suggest that the major cause of the changes in the diffusion MR signals is the strong depolarization of the neurons.

However, changes in the diffusion MR signals, whereas strongly dependent on the prolonged depolarization levels, were independent of the level of normal neuronal spikes. In our kainate concentration experiments, changes in the diffusion-weighted signals diminished as the prolonged depolarization level decreased during the reduction of kainate concentration, whereas the number of neuronal spikes in the population increased. A similar result was found in our PTX experiments, in which significant diffusion MR signal changes were only found at the higher PTX concentration that clearly elicited a prolonged depolarization. In the TTX experiments, the suppression of normal spontaneous neuronal activity had no observable effect on the diffusion MR signals. In control experiments without a drug application, no evidence was found that each single event of normal neuronal activity induced significant changes in the highly diffusion-weighted MR signals ($b = 1{,}800$ s/mm^2) within a temporal resolution of 100 ms.

Organotypic cultures represent an in vitro model in which a slab of cortical tissue can be kept alive and active for many weeks. Anatomical studies have shown that these cultures maintain all major cell types and cortical layer characteristics as in vivo (22, 23). Importantly, the neuronal activity in this in vitro system is found to organize into active 0.5- to 3-s-long periods (up-states) separated by up to 10 s of very low activity (down-states). Comparison of intracellular and extracellular spike activity demonstrated that during up-state periods, all neurons are depolarized and pyramidal neurons display average firing rates of ~1 Hz, typical found for resting activity in vivo (24, 48). In fact, the spatiotemporal organization of the neuronal population activity during up-states (25, 28) is characteristic of neuronal avalanches, the resting state organization identified in vivo in rodents, nonhuman primates (27), and humans (49). We therefore conclude that up-state activity measured in organotypic cultures best matches ongoing resting activity in vivo. Similarly, evoked activity in this in vitro system (24, 50) mimics evoked activity in vivo, e.g., barrel cortex in awake mice (51). Interestingly, experiments demonstrated that evoked activity by a sensory stimulus in vivo (52) or electric stimulation in vitro (50) only weakly modulates the ongoing resting neuronal activity, which suggests the diffusion MRI might also not be sensitive enough to capture the evoked neuronal activity in most functional MRI studies. In short, the synchronous bursting behavior of the neurons in our experiment represents a "best case" scenario for being able to detect neuronal activity via MR methods. Less synchronized, less coherent neuronal responses would be less detectable.

In this study, five *b*-values ranging from 0 to 2,400 s/mm^2 with a step of 600 s/mm^2 were applied and fitted with a bicomponent model; the *b*-values and fitting procedure were similar to those in previous fDMRI studies (10, 14, 18). In the 100 μM kainate experiments, the diffusion MR data were also fitted with Eq. **1** without D_{fast} and D_{slow} fixed during and after drug application; the fitting results didn't reveal any significant changes in the two diffusion constants. The results agree with the previous work (10) and make it reasonable to fix D_{fast} and D_{slow} with values from predrug MR data to reduce the fitting uncertainty.

Here both the slow diffusion component fraction *f* and its changes (under 100 μM kainate and 30 mM K^+) are smaller than the results from acute rat adult brain slices with imaging (14). This difference might be the result of the partial-volume effect here [the cultures can only occupy ~50–60% of the detective volume inside the radio frequency (RF) coil, see more discussion in ref. 21]. The large portion of the ACSF inside the RF detective volume would be counted as a part of the fast diffusion component, which can

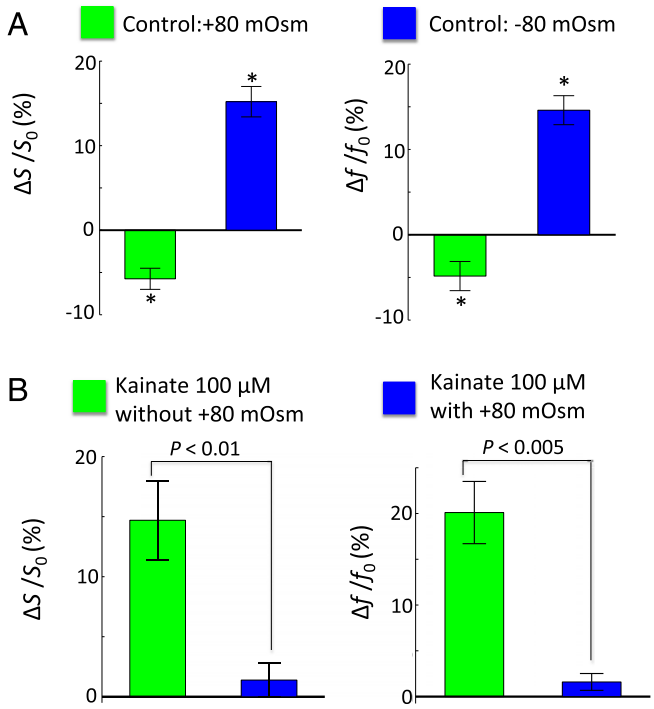

Fig. 7. Osmotic pressure challenge experiments. (*A*) The normalized changes in the diffusion-weighted MR signals (the average of the MR signals at b =1,800 and 2,400 s/mm^2; *Left*) and the slow diffusion coefficients (*Right*) in +80 and −80 mOsm ACSF in control experiments without kainate. (*B*) The normalized changes in the diffusion-weighted MR signals (the average of the MR signals at b = 1,800 and 2,400 s/mm^2; *Left*) and the slow diffusion coefficients (*Right*) in the 100 μM kainate application with and without +80 mOsm challenge. *$P < 0.05$ with Student's t test.

also explain the relatively larger D_{fast} obtained here than that observed in vivo using the same bicomponent model (33, 53). On the other hand, the ADC of the slow diffusion component, D_{slow}, which might arise from intracellular water, observed here falls in the same range as the in vivo results (33, 53). Interestingly, the diffusion MR signals will also change as the brain development in animals or humans, and the f obtained from the organotypic cortical cultures, which were incubated from neonatal rat brain cortex, is close to that obtained from neonatal rat brain cortex in vivo (f = 11 ± 1%) (54). In addition, the diffusion time in the diffusion MR sequence used here (≤0.4 ms) is much shorter than that in the conventional fDMRI experiments (∼80 ms for clinical scanners and ∼10–30 ms for preclinical scanners) (10, 11, 14–16). It has been reported that diffusion MR signals from the cortex are strongly dependent on diffusion time, especially at short diffusion time (≤10 ms) (53, 55). The further discussion about diffusion-time dependence in the resting and active states is beyond the scope of this article but an interesting direction for future investigation. Although differences exist between this in vitro system and the in vivo case, similar findings in the stroke model as in vivo studies provide additional evidence that the organotypic culture system mimics well-known behaviors observed in mammalian brains in vivo.

A phenomenon of cell swelling induced by intense neuronal depolarization has been reported in other imaging studies (37, 44, 56–60). Cell volume changes have also been reported in ischemia, stroke (Fig. 8), osmotic modulation, and spreading depression (37, 42, 44, 57); in all of these instances, diffusion-weighted MRI shows a positive response (40, 41, 61). Thus, cell swelling may contribute to the reduced water diffusivity observed here and in other pathological states mentioned above. The contribution of cell swelling was further studied with osmotic pressure experiments on the organotypic cultures (Fig. 7). In the control, the diffusion-weighted MR signals decreased at +80 mOsm and increased at −80 mOsm. The +80-mOsm challenge during the perfusion of 100 μM kainate induced significant recovery in the diffusion MR signals caused by the depolarization block; this result suggests that cell swelling counts, at least in part, for the reduced water diffusivity observed during cell depolarization, although other mechanisms may be at work as well. The biophysical basis of bicomponent diffusion in the living cortex is still unclear, and further investigations about how cell swelling induces the increase of the slow diffusion component fraction is beyond the scope of this article. Here we offer some possible mechanisms proposed by other groups, which include, but are not limited to (*i*) an increase of diffusion tortuosity in the extracellular space and intracellular volume fraction (62); (*ii*) more "bound" water near the lipid membrane with slow diffusivity during cell swelling (33, 63); and (*iii*) changes in the configuration of the cytoplasmic matrix and streaming (64).

Cell swelling has also been reported to occur during normal neuronal activity, but with a negligible amplitude that is much smaller than that caused by prolonged and strong depolarization (44, 56, 65–68). In general, the displacements of the cell surface are on the length scale of nanometers, with a maximum displacement of several tens of nanometers, under normal electrical stimulation (65–68). However, the surface displacement changes in the neuronal soma induced by prolonged depolarization can be ≥∼1 μm (44, 56, 57). Therefore, it is unlikely that diffusion MRI is sensitive enough to measure the minor changes caused by normal neuronal activity, which are several orders of magnitude smaller than the changes observed in prolonged depolarization. Moreover, the timescale of most physiological processes that occur during single neuronal activation events, such as action potential firing, ion exchange, channel opening and closing, cell swelling, and other mechanical changes, is several tens of milliseconds or less (47, 68) and shorter than typical diffusion MRI experiments. Thus, current diffusion MR techniques may not be fast enough to capture single events of neuronal activity/spikes even if we assume they can affect water diffusion.

Diffusion MR signals arise from water molecules within the extracellular matrix and cells including neurons, astrocytes, and microglial cells. The relationship between the observed diffusion MR signals and the underlying microstructure, composition, and water dynamics is still poorly understood. In addition to neuronal cell swelling, other active physiological processes can also contribute to the changes in the diffusion MR signals. Morphological studies showed that the neuronal cell membrane might become "leaky" under intense excitation (44, 59); this cell membrane permeability change might modulate water exchange between compartments and change the diffusion MR signals (69). It has also been suggested that changes in the microstreaming (local advection) might change the diffusion MR signal through pseudo-diffusion (16, 70). In addition, astrocytes and other glial cells could also play a role in brain water dynamics (71); their contribution to the diffusion MR signal is still not clear.

In summary, simultaneous intracellular calcium imaging and diffusion MR measurements clearly demonstrate a direct correlation between reduced water diffusivity and depolarization of the neuronal cell membrane in conditions of neuronal hyperexcitability. These changes in diffusion MR signals are positively correlated only with the amplitude of prolonged depolarization rather than with the levels of normal spontaneous neuronal activity. Nonetheless, these findings are consistent with findings in clinical and preclinical diffusion MRI when used to monitor related brain disorders. Currently, fDMRI does not seem to be able to track normal neuronal activity in our system, either in terms of sensitivity or temporal resolution. Our results suggest that observed diffusion fMRI changes during some functional tasks in vivo might be

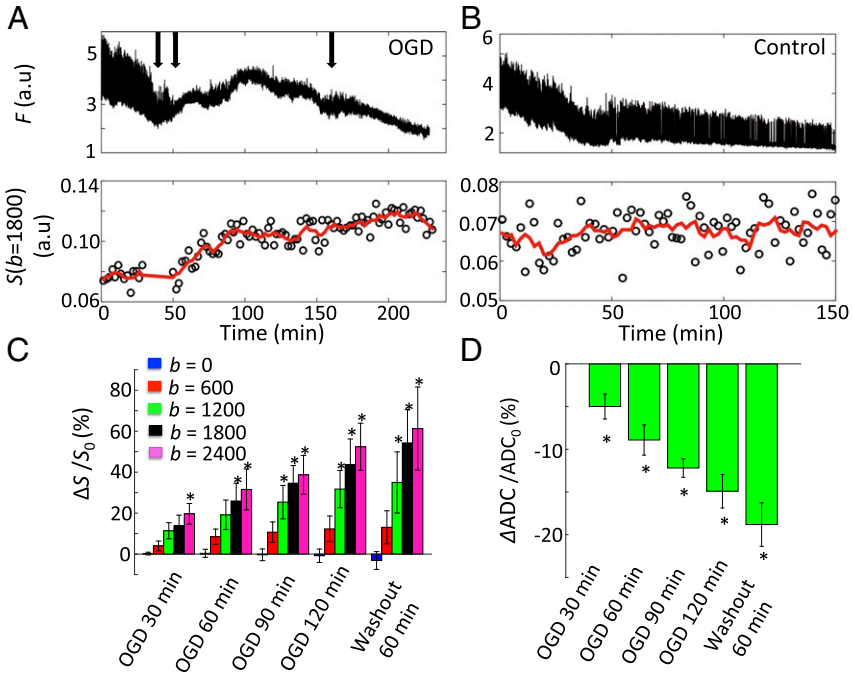

Fig. 8. OGD stroke model. (*A* and *B*) The calcium fluorescence signal (*Upper*) and the diffusion MR signal at $b = 1{,}800$ s/mm^2 (*Lower*) in the response of OGD (*A*) and normal ACSF (*B*, control). Red continuous curve: sliding data average (six data points each). The three black arrows in *A* indicate the state of the faster OGD perfusion, normal OGD perfusion, and washout with normal ACSF, respectively. (*C*) Changes in the diffusion MR signals at various *b*-values and various OGD times. (*D*) Changes in ADC at various OGD times. $^*P < 0.05$ with Student's *t* test for MR results.

artifactual to a certain degree, originating most likely from vascular coupling rather than from the direct effects of neuronal activity.

Materials and Methods

Preparation of Organotypic Rat Cortical Cultures. The organotypic tissue cultures were made from somatosensory cortex from acute coronal slices of newborn rats (postnatal day 0–2; Sprague–Dawley). Two acute slices (350 μm thick) were attached to the #1 coverslip by using a plasma-thrombin mixture, submerged in 800 μL culture medium, and incubated at 35.0 ± 0.5 °C. The medium was replaced every 3–4 d. Cultures were grown for 2–3 wk before being used in experiments (for details, see refs. 72 and 73).

Simultaneous Calcium Optical Imaging and Diffusion MR. A detailed description of this optical-MR hybrid system, which enables simultaneous fluorescence imaging and MR measurements, is provided in ref. 21. Briefly, a single-sided MR "profiler" with open access was mounted under the stage of a fluorescence microscope with an objective having a long working distance. A custom environmental chamber was mounted between the two imaging systems, in which optical images were acquired from above the culture and the MR signals were acquired from below the culture. The environmental chamber was used to maintain the organotypic cortex culture's oxygen, ACSF perfusion, temperature, etc. The cultures were incubated with 50 μM OGB (Life Technologies) for 1–2 h before the experiments were performed. A GFP fluorescence filter unit (Olympus America) and a color CCD camera (ProgRes CF scan; Jenoptik) were used to acquire the real-time fluorescence images.

The single-sided MR system consists of four permanent magnets, which generate a uniform magnetic field (0.32 T, 15 × 15 mm) in a plane parallel to the microscope stage ∼15 mm from the top surface of the magnets (31, 74). A custom multiturn double-layered RF surface coil with an inner diameter of 5 mm was mounted directly below the tissue slide, matching the size of the cortex cultures. This design reduces the partial volume effect and improves the sensitivity of the MR signal detection. In this study, MR spectroscopy data were acquired without imaging. Diffusion weighting was achieved by varying the echo time in a spin echo (SE) sequence in the presence of a static constant magnetic gradient ($G_0 = 650$ kHz/mm) (21, 31). The direction of the static magnetic gradient is perpendicular to the plane of the culture slices. Following diffusion weighting, Carr–Purcell–Meiboom–Gill (CPMG) echo trains were generated and collected to improve MR sensitivity. An add/subtract phase cycle of the first 90° excitation pulse was implemented to eliminate the baseline drift artifacts. The detailed sequence and the definition of the *b*-values can be found in figure 2 and equation 4 of ref. 21.

Experimental Protocol. In these experiments, the organotypic cortex culture was kept in the environmental chamber with constant and slow perfusion (30 mL/h) of oxygenated [95% (vol/vol) O_2 + 5% (vol/vol) CO_2] ACSF (124 mM NaCl, 3.5 mM KCl, 10 mM glucose, 26.2 mM $NaHCO_3$, 0.3 mM NaH_2PO_4, 1.2 mM $CaCl_2$, and 1 mM $MgSO_4$). Temperature was kept constant at 34.0 ± 1.0 °C. During the kainate, PTX, and TTX experiments, these agents were added directly into the ACSF feed stream at the given concentrations. As for the extracellular K^+ experiments, the concentration of NaCl was reduced to maintain a constant osmotic pressure (292–296 mOsm). A 10-min drug perfusion was added in the middle of normal ACSF perfusion for each drug.

In the osmotic pressure challenge experiments, the osmotic pressure of the ACSF was increased and decreased by 80 mOsm by direct addition of mannitol or distilled water to the normal ACSF, respectively (37). In the control experiments, the following experimental protocol was performed: normal ACSF (30 min) → +80 mOsm (15 min) → normal ACSF (30 min) → -80 mOsm (15 min) → normal ACSF. The last 10-min diffusion MR data following the osmotic modulation were selected and averaged to compare with the initial state. To study the effect of the osmotic pressure on the kainate-induced diffusion MR changes, experiments were performed following the protocol: normal ACSF (20 min) → 100 μM kainate under +80 mOsm (10 min) → normal ACSF (30 min) → 100 μM kainate under normal osmotic pressure (10 min) → normal ACSF.

During the experiments, calcium images were acquired with 1× magnification, 8.8 × 6.6 mm field of view (FOV), 680 × 512 pixels, exposure of 100 ms, and 10 frames/s. As for the diffusion MR, five *b*-values ranging from 0 to 2,400 s/mm^2 with a step of 600 s/mm^2 were acquired with two-step phase cycling, TR = 2 s, 2,000 echoes with an echo time of 40 μs, and a slice thickness of 100 μm. For the time profile experiments without a pathological drug application, diffusion MR data were acquired at a single *b*-value ($b = 1{,}800$ s/mm^2) with all of the other settings kept the same as described above.

Signal Processing. The calcium signal (*F*) was defined as the average fluorescence signal inside a region of interest (ROI), which was drawn to contain all cortical tissues within the bounds of the RF coil. Background subtraction was performed on *F* by automatically subtracting the signal from a manually defined background ROI containing no tissue. The baseline F_0 of *F* was

calculated using a 30-s sliding window. In the time profile experiments, fluorescence values were then expressed as a relative percentage change with respect to the baseline, $\%\Delta F/F_0$, and a 1D deconvolution algorithm was implemented to detect the time of the peak neuronal activity. Details and examples are provided in ref. 21.

As for the diffusion MR acquisition, the first four echoes in each CPMG echo train, which had systematic artifacts, were removed (74). Then the average of the entire CPMG echo train was used as the signal intensity at each *b*-value. In the studies in which pharmacological agents were added, the diffusion signals from the 10-min preadministration state in each sample were averaged and fitted with Eq. **1** at first. Then, the 10 min of data acquired during drug application and during the postdrug state were averaged and fitted with Eq. **1** with fixed D_{fast} and D_{slow} obtained from the predrug results.

Time-Series Analysis of the Calcium Signal and Diffusion-Weighted MR Signals Without a Drug Application. Here, 16 organotypic cortical samples were scanned at a single *b*-value (b =1,800 s/mm^2) under normal ACSF conditions with no drug application (1.5–3.0 h of continuous recording). Periods of high (active) and low (resting) neuronal activity were identified in the intracellular calcium signal, and the MR signal was binned into these two categories on the basis of its recording time. Two types of time-series analysis methods were developed and tested here. For the first type (Type 1), we hypothesized that each neuronal population activity event would only affect the diffusion MR signal (active) recorded immediately after it (the starting time of the neuronal event) within a time window, *T*, which was varied over a range from $T = 0.1$ to 1.0 s in steps of 0.1 s. The corresponding resting MR signal for each active MR signal was the MR data recorded closest in time before the neuronal event (Fig. 6*A*). For the second type of time-series analysis (Type 2), we hypothesized that each neuronal population activity event would only affect the MR signal (active) recorded within 1 s before and following it (the starting time of the neuronal event). All MR signals outside of this 2-s time window were denoted as resting state (Fig. 6*B*). The active MR signals were further binned into groups on the basis of how separate they were in time (Δ) from the neuronal event with a time step of 0.1 s. For each active MR, the four resting MRs closest to it in time, both before and after, were chosen and averaged as the corresponding resting MR.

In the Type 1 analysis, paired Student's *t* tests were performed on the results from all 16 specimens with the null hypothesis that the mean of the active MR signals would be larger than the resting MR signals. For the Type 2 analysis, similar Student's *t* tests were performed on the paired comparisons between the active (the entire 2-s time window without further binning) and resting MR signals. One-way ANOVA was also performed on the time-profile MR results with the null hypothesis that the mean of the changes between active and resting MR in each bin (Δ) would be equal.

All of the signal postprocessing and analyses were implemented in MATLAB.

ACKNOWLEDGMENTS. We thank Prof. Robert M. Briber (University of Maryland) for lively discussions and helpful suggestions; Drs. Andreas Klaus, Timothy Bellay, and Hellmut Merkle (National Institutes of Health) and Dr. Uri Nevo (Tel-Aviv University) for help in setting up the hybrid test system; Dr. Sinisa Pajevic (Center for Information Technology, NIH) for useful discussions about time series analysis; our colleague Dr. Carlo Pierpaoli for insightful comments; and Ms. Liz Salak for editing the manuscript. This work was supported by the Intramural Research Program of the Eunice Kennedy Shriver National Institute of Child Health and Human Development, NIH.

1. Kwong KK, et al. (1992) Dynamic magnetic resonance imaging of human brain activity during primary sensory stimulation. *Proc Natl Acad Sci USA* 89(12):5675–5679.
2. Ogawa S, et al. (1992) Intrinsic signal changes accompanying sensory stimulation: Functional brain mapping with magnetic resonance imaging. *Proc Natl Acad Sci USA* 89(13):5951–5955.
3. Bandettini PA, Wong EC, Hinks RS, Tikofsky RS, Hyde JS (1992) Time course EPI of human brain function during task activation. *Magn Reson Med* 25(2):390–397.
4. Logothetis NK (2007) The ins and outs of fMRI signals. *Nat Neurosci* 10(10):1230–1232.
5. Logothetis NK (2008) What we can do and what we cannot do with fMRI. *Nature* 453(7197):869–878.
6. Bandettini PA (2009) Seven topics in functional magnetic resonance imaging. *J Integr Neurosci* 8(3):371–403.
7. Le Bihan D, Breton E (1985) Imagerie de diffusion in-vivo par résonance magnétique nucléaire. *Comptes Rendus Acad Sci* 93(5):27–34.
8. Merboldt K-D, Hanicke W, Frahm J (1985) Self-diffusion NMR imaging using stimulated echoes. *J Magn Reson* 64(3):479–486.
9. Taylor DG, Bushell MC (1985) The spatial mapping of translational diffusion coefficients by the NMR imaging technique. *Phys Med Biol* 30(4):345–349.
10. Le Bihan D, Urayama S, Aso T, Hanakawa T, Fukuyama H (2006) Direct and fast detection of neuronal activation in the human brain with diffusion MRI. *Proc Natl Acad Sci USA* 103(21):8263–8268.
11. Tsurugizawa T, Ciobanu L, Le Bihan D (2013) Water diffusion in brain cortex closely tracks underlying neuronal activity. *Proc Natl Acad Sci USA* 110(28): 11636–11641.
12. Zhong J, Petroff OAC, Pleban LA, Gore JC, Prichard JW (1997) Reversible, reproducible reduction of brain water apparent diffusion coefficient by cortical electroshocks. *Magn Reson Med* 37(1):1–6.
13. Darquié A, Poline JB, Poupon C, Saint-Jalmes H, Le Bihan D (2001) Transient decrease in water diffusion observed in human occipital cortex during visual stimulation. *Proc Natl Acad Sci USA* 98(16):9391–9395.
14. Flint J, Hansen B, Vestergaard-Poulsen P, Blackband SJ (2009) Diffusion weighted magnetic resonance imaging of neuronal activity in the hippocampal slice model. *Neuroimage* 46(2):411–418.
15. Bui JD, Buckley DL, Phillips MI, Blackband SJ (1999) Nuclear magnetic resonance imaging measurements of water diffusion in the perfused hippocampal slice during N-methyl-D-aspartate-induced excitotoxicity. *Neuroscience* 93(2):487–490.
16. Tirosh N, Nevo U (2013) Neuronal activity significantly reduces water displacement: DWI of a vital rat spinal cord with no hemodynamic effect. *Neuroimage* 76:98–107.
17. Jin T, Kim S-G (2008) Functional changes of apparent diffusion coefficient during visual stimulation investigated by diffusion-weighted gradient-echo fMRI. *Neuroimage* 41(3):801–812.
18. Miller KL, et al. (2007) Evidence for a vascular contribution to diffusion FMRI at high b value. *Proc Natl Acad Sci USA* 104(52):20967–20972.
19. Autio JAA, et al. (2011) High b-value diffusion-weighted fMRI in a rat forepaw electrostimulation model at 7 T. *Neuroimage* 57(1):140–148.
20. Jin T, Zhao F, Kim S-G (2006) Sources of functional apparent diffusion coefficient changes investigated by diffusion-weighted spin-echo fMRI. *Magn Reson Med* 56(6): 1283–1292.
21. Bai R, et al. (2015) Simultaneous calcium fluorescence imaging and MR of ex vivo organotypic cortical cultures: A new test bed for functional MRI. *NMR Biomed* 28(12): 1726–1738.
22. Caeser M, Schüz A (1992) Maturation of neurons in neocortical slice cultures: A light and electron microscopic study on in situ and in vitro material. *J Hirnforsch* 33(4-5): 429–443.
23. Plenz D, Aertsen A (1996) Neural dynamics in cortex-striatum co-cultures–I. anatomy and electrophysiology of neuronal cell types. *Neuroscience* 70(4):861–891.
24. Plenz D, Aertsen A (1996) Neural dynamics in cortex-striatum co-cultures–II. Spatiotemporal characteristics of neuronal activity. *Neuroscience* 70(4):893–924.
25. Beggs JM, Plenz D (2003) Neuronal avalanches in neocortical circuits. *J Neurosci* 23(35):11167–11177.
26. Gireesh ED, Plenz D (2008) Neuronal avalanches organize as nested theta- and beta/gamma-oscillations during development of cortical layer 2/3. *Proc Natl Acad Sci USA* 105(21):7576–7581.
27. Petermann T, et al. (2009) Spontaneous cortical activity in awake monkeys composed of neuronal avalanches. *Proc Natl Acad Sci USA* 106(37):15921–15926.
28. Bellay T, Klaus A, Seshadri S, Plenz D (2015) Irregular spiking of pyramidal neurons organizes as scale-invariant neuronal avalanches in the awake state. *eLife* 4: e07224.
29. Berridge MJ, Lipp P, Bootman MD (2000) The versatility and universality of calcium signalling. *Nat Rev Mol Cell Biol* 1(1):11–21.
30. Tsien RW, Tsien RY (1990) Calcium channels, stores, and oscillations. *Annu Rev Cell Biol* 6:715–760.
31. Rata DG, Casanova F, Perlo J, Demco DE, Blümich B (2006) Self-diffusion measurements by a mobile single-sided NMR sensor with improved magnetic field gradient. *J Magn Reson* 180(2):229–235.
32. Le Bihan D (1995) Molecular diffusion, tissue microdynamics and microstructure. *NMR Biomed* 8(7-8):375–386.
33. Le Bihan D (2007) The 'wet mind': Water and functional neuroimaging. *Phys Med Biol* 52(7):R57–R90.
34. Henkelman RM, Stanisz GJ, Kim JK, Bronskill MJ (1994) Anisotropy of NMR properties of tissues. *Magn Reson Med* 32(5):592–601.
35. Buckley DL, et al. (1999) The effect of ouabain on water diffusion in the rat hippocampal slice measured by high resolution NMR imaging. *Magn Reson Med* 41(1): 137–142.
36. Shew WL, Yang H, Yu S, Roy R, Plenz D (2011) Information capacity and transmission are maximized in balanced cortical networks with neuronal avalanches. *J Neurosci* 31(1):55–63.
37. Andrew RDD, MacVicar BA (1994) Imaging cell volume changes and neuronal excitation in the hippocampal slice. *Neuroscience* 62(2):371–383.
38. Mintorovitch J, et al. (1991) Comparison of diffusion- and T2-weighted MRI for the early detection of cerebral ischemia and reperfusion in rats. *Magn Reson Med* 18(1): 39–50.
39. Moseley ME, et al. (1990) Diffusion-weighted MR imaging of acute stroke: Correlation with T2-weighted and magnetic susceptibility-enhanced MR imaging in cats. *AJNR Am J Neuroradiol* 11(3):423–429.
40. Baird AE, Warach S (1998) Magnetic resonance imaging of acute stroke. *J Cereb Blood Flow Metab* 18(6):583–609.
41. van Pul C, Jennekens W, Nicolay K, Kopinga K, Wijn PFF (2005) Ischemia-induced ADC changes are larger than osmotically-induced ADC changes in a neonatal rat hippocampus model. *Magn Reson Med* 53(2):348–355.
42. Dirnagl U, Iadecola C, Moskowitz MA (1999) Pathobiology of ischaemic stroke: An integrated view. *Trends Neurosci* 22(9):391–397.

43. Choi DW (1988) Calcium-mediated neurotoxicity: Relationship to specific channel types and role in ischemic damage. *Trends Neurosci* 11(10):465–469.
44. Andrew RD, Labron MW, Boehnke SE, Carnduff L, Kirov SA (2007) Physiological evidence that pyramidal neurons lack functional water channels. *Cereb Cortex* 17(4): 787–802.
45. Berdichevsky E, Riveros N, Sánchez-Armáss S, Orrego F (1983) Kainate, N-methyl-aspartate and other excitatory amino acids increase calcium influx into rat brain cortex cells in vitro. *Neurosci Lett* 36(1):75–80.
46. Robinson JH, Deadwyler SA (1981) Kainic acid produces depolarization of CA3 pyramidal cells in the vitro hippocampal slice. *Brain Res* 221(1):117–127.
47. Bear MF, Connors BW, Paradiso MA (2007) Neuroscience (Lippincott Williams & Wilkins, Baltimore), 3rd Ed.
48. Plenz D, Kitai ST (1998) Up and down states in striatal medium spiny neurons simultaneously recorded with spontaneous activity in fast-spiking interneurons studied in cortex-striatum-substantia nigra organotypic cultures. *J Neurosci* 18(1):266–283.
49. Shriki O, et al. (2013) Neuronal avalanches in the resting MEG of the human brain. *J Neurosci* 33(16):7079–7090.
50. Shew WL, Yang H, Petermann T, Roy R, Plenz D (2009) Neuronal avalanches imply maximum dynamic range in cortical networks at criticality. *J Neurosci* 29(49):15595–15600.
51. Poulet JFA, Petersen CCH (2008) Internal brain state regulates membrane potential synchrony in barrel cortex of behaving mice. *Nature* 454(7206):881–885.
52. Fiser J, Chiu C, Weliky M (2004) Small modulation of ongoing cortical dynamics by sensory input during natural vision. *Nature* 431(7008):573–578.
53. Pyatigorskaya N, Le Bihan D, Reynaud O, Ciobanu L (2014) Relationship between the diffusion time and the diffusion MRI signal observed at 17.2 Tesla in the healthy rat brain cortex. *Magn Reson Med* 72(2):492–500.
54. Niendorf T, Dijkhuizen RM, Norris DG, van Lookeren Campagne M, Nicolay K (1996) Biexponential diffusion attenuation in various states of brain tissue: Implications for diffusion-weighted imaging. *Magn Reson Med* 36(6):847–857.
55. Niendorf T, Norris DG, Leibfritz D (1994) Detection of apparent restricted diffusion in healthy rat brain at short diffusion times. *Magn Reson Med* 32(5):672–677.
56. Risher WC, Andrew RD, Kirov SA (2009) Real-time passive volume responses of astrocytes to acute osmotic and ischemic stress in cortical slices and in vivo revealed by two-photon microscopy. *Glia* 57(2):207–221.
57. Zhou N, Gordon GRJ, Feighan D, MacVicar BA (2010) Transient swelling, acidification, and mitochondrial depolarization occurs in neurons but not astrocytes during spreading depression. *Cereb Cortex* 20(11):2614–2624.
58. Choi DW (1992) Excitotoxic cell death. *J Neurobiol* 23(9):1261–1276.
59. Maulucci-Gedde M, Choi DW (1987) Cortical neurons exposed to glutamate rapidly leak preloaded 51chromium. *Exp Neurol* 96(2):420–429.
60. Meyer FB (1989) Calcium, neuronal hyperexcitability and ischemic injury. *Brain Res Brain Res Rev* 14(3):227–243.
61. Busch E, Gyngell ML, Eis M, Hoehn-Berlage M, Hossmann KA (1996) Potassium-induced cortical spreading depressions during focal cerebral ischemia in rats: Contribution to lesion growth assessed by diffusion-weighted NMR and biochemical imaging. *J Cereb Blood Flow Metab* 16(6):1090–1099.
62. Latour LL, Svoboda K, Mitra PP, Sotak CH (1994) Time-dependent diffusion of water in a biological model system. *Proc Natl Acad Sci USA* 91(4):1229–1233.
63. Pollack GH (2001) *Cells, Gels and the Engines of Life: A New, Unifying Approach to Cell Function* (Ebner & Sons, Seattle).
64. Dijkhuizen RM, de Graaf RA, Tulleken KA, Nicolay K (1999) Changes in the diffusion of water and intracellular metabolites after excitotoxic injury and global ischemia in neonatal rat brain. *J Cereb Blood Flow Metab* 19(3):341–349.
65. Iwasa K, Tasaki I, Gibbons R (1980) Swelling of nerve fibers associated with action potentials. *Science* 210(4467):338–339.
66. Tasaki I, Iwasa K (1982) Rapid pressure changes and surface displacements in the squid giant axon associated with production of action potentials. *Jpn J Physiol* 32(1):69–81.
67. Tasaki I, Byrne PM (1992) Rapid structural changes in nerve fibers evoked by electric current pulses. *Biochem Biophys Res Commun* 188(2):559–564.
68. Tasaki I (1999) Rapid structural changes in nerve fibers and cells associated with their excitation processes. *Jpn J Physiol* 49(2):125–138.
69. Lee J-HH, Springer CS, Jr (2003) Effects of equilibrium exchange on diffusion-weighted NMR signals: The diffusigraphic "shutter-speed". *Magn Reson Med* 49(3): 450–458.
70. Nevo U, et al. (2010) A system and mathematical framework to model shear flow effects in biomedical DW-imaging and spectroscopy. *NMR Biomed* 23(7):734–744.
71. Fields RD, Woo DH, Basser PJ (2015) Glial regulation of the neuronal connectome through local and long-distant communication. *Neuron* 86(2):374–386.
72. Stewart CV, Plenz D (2008) Homeostasis of neuronal avalanches during postnatal cortex development in vitro. *J Neurosci Methods* 169(2):405–416.
73. Plenz D, et al. (2011) Multi-electrode array recordings of neuronal avalanches in organotypic cultures. *J Vis Exp* (54):2949, 10.3791/2949.
74. Casanova F, Perlo J, Blümich B (2011) *Single-Sided NMR* (Springer, Berlin).

Supporting Information

Bai et al. 10.1073/pnas.1519890113

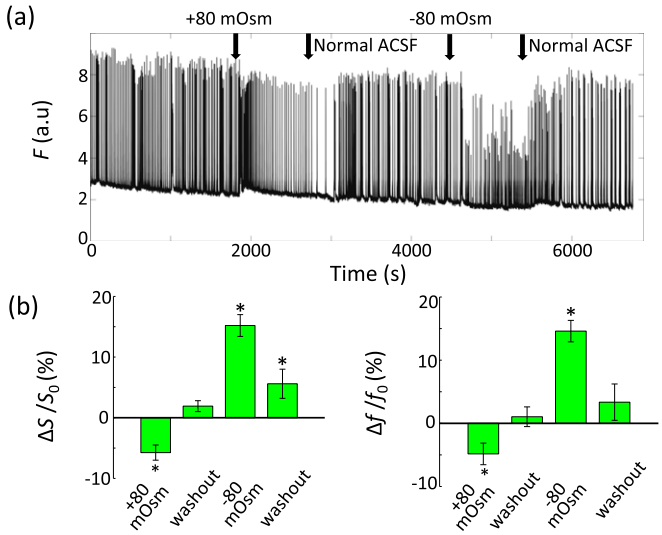

Fig. S1. Osmotic pressure modulation in control experiments. (*A*) The calcium fluorescence signal and (*B*) the normalized changes in the diffusion-weighted MR signals (the average of the MR signals at b = 1,800 and 2,400 s/mm^2; *Left*) and the slow diffusion coefficients (*Right*) in the response of the osmotic pressure modulation with experimental protocol: normal ACSF (30 min) → +80 mOsm (15 min) → normal ACSF (30 min) → -80 mOsm (15 min) → normal ACSF. *P < 0.05 with Student's t test for MR results.

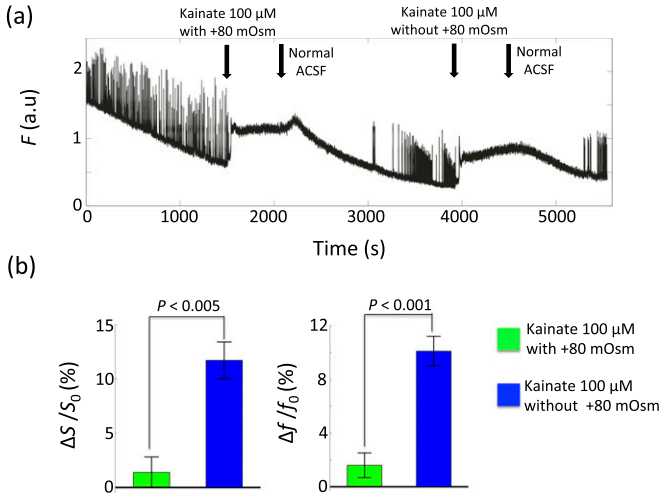

Fig. S2. Osmotic pressure modulation during depolarization block. (*A*) The calcium fluorescence signal and (*B*) the normalized changes in the diffusion-weighted MR signals (the average of the MR signals at b = 1,800 and 2,400 s/mm^2; *Left*) and the slow diffusion coefficients (*Right*) in the response to the perfusion of kainate 100 μM with and without +80 mOsm challenge, with the experimental protocol: normal ACSF (20 min) → kainate 100 μM with +80 mOsm challenge (10 min) → normal ACSF (30 min) → kainate 100 μM without +80 mOsm challenge (10 min) → normal ACSF.